

**ACCEPTED MANUSCRIPT**

## Magnetic anisotropy and Curie temperature of two-dimensional VI<sub>3</sub> monolayer

To cite this article before publication: Fazle Subhan *et al* 2020 *J. Phys.: Condens. Matter* in press <https://doi.org/10.1088/1361-648X/ab7c14>

### Manuscript version: Accepted Manuscript

Accepted Manuscript is “the version of the article accepted for publication including all changes made as a result of the peer review process, and which may also include the addition to the article by IOP Publishing of a header, an article ID, a cover sheet and/or an ‘Accepted Manuscript’ watermark, but excluding any other editing, typesetting or other changes made by IOP Publishing and/or its licensors”

This Accepted Manuscript is © 2020 IOP Publishing Ltd.

During the embargo period (the 12 month period from the publication of the Version of Record of this article), the Accepted Manuscript is fully protected by copyright and cannot be reused or reposted elsewhere.

As the Version of Record of this article is going to be / has been published on a subscription basis, this Accepted Manuscript is available for reuse under a CC BY-NC-ND 3.0 licence after the 12 month embargo period.

After the embargo period, everyone is permitted to use copy and redistribute this article for non-commercial purposes only, provided that they adhere to all the terms of the licence <https://creativecommons.org/licenses/by-nc-nd/3.0>

Although reasonable endeavours have been taken to obtain all necessary permissions from third parties to include their copyrighted content within this article, their full citation and copyright line may not be present in this Accepted Manuscript version. Before using any content from this article, please refer to the Version of Record on IOPscience once published for full citation and copyright details, as permissions will likely be required. All third party content is fully copyright protected, unless specifically stated otherwise in the figure caption in the Version of Record.

View the [article online](#) for updates and enhancements.

1  
2  
3 Magnetic Anisotropy and Curie Temperature of Two-Dimensional VI<sub>3</sub> Monolayer  
45 Fazole Subhan and Jisang Hong\*  
67 Department of Physics, Pukyong National University, Busan 48513, Korea.  
8  
9  
10  
11**ABSTRACT**

13 Recently, it was reported that the VI<sub>3</sub> had Mott insulator nature and also displayed the structural and magnetic phase  
14 transition at low temperature. Here, we explored the magnetic properties of the two-dimensional (2D) monolayer  
15 structure using the density functional theory (DFT). We found that the 2D VI<sub>3</sub> had an enhanced lattice constant  
16 compared with that in the bulk structure. Besides, the 2D monolayer had an indirect band gap of 0.98 eV, and this  
17 band gap was increased (decreased) with tensile (compressive) strain up to  $\pm 3\%$ . The monolayer structure had a  
18 ferromagnetic ground state and this nature was preserved under both tensile and compressive strains. We obtained that  
19 the monolayer structure had a perpendicular magnetic anisotropy energy of 0.29 meV/cell. The perpendicular  
20 magnetic anisotropy still remained even after applying the tensile and compressive strains although the magnitude of  
21 magnetic anisotropy was slightly changed. Using the Metropolis Monte Carlo (MC) simulations, we found that the  
22 monolayer had a Curie temperature of 46 K. This Curie temperature was increased to 57 K with 3 % tensile strain  
23 whereas it was decreased to 35 K with 3 % compressive strain. Overall, we found that the magnetic property of 2D  
24 VI<sub>3</sub> monolayer was robust under the strain.

25  
26  
27  
28  
29  
30  
31  
32  
33  
34  
35  
36  
37  
38

**Corresponding Author**41 \*E-mail: [hongj@pknu.ac.kr](mailto:hongj@pknu.ac.kr)

### INTRODUCTION

Two-dimensional (2D) van der Waals (vdW) materials display many intriguing physical properties and these offer an exciting platform for technological breakthroughs for novel device applications in diverse fields. Therefore, the study on 2D materials has become one of the most attracting subjects in condensed matter physics and material sciences. Indeed, the successful isolation of graphene[1] triggered extensive research efforts on 2D materials, and a wide variety of 2D materials such as transition metal dichalcogenides (TMDs), hexagonal boron nitride (hBN), silicene and black phosphorous have been fabricated in the last several years [2–4]. In these materials, the diverse physical properties have been investigated such as electronic band structures, optoelectronics, valleytronics, or Rashba effect[1,5–10]. However, most of the previously available 2D materials are non-magnetic in their pristine forms, and this nature limits the potential spintronics applications [11–13].

Stimulated by the rich physics observed in the non-magnetic 2D materials, the recent study has been focused on the 2D magnetic materials. Regarding the magnetic properties of the 2D materials, numerous theoretically designed 2D magnetic materials have been proposed using the density functional calculations and also molecular dynamics by checking their structural stability. Nonetheless, only a few intrinsic 2D magnetic materials have been successfully synthesized experimentally so far. The most well-known experimentally fabricated 2D magnetic materials are CrI<sub>3</sub>,[14–16] CrGeTe<sub>3</sub> [17], and Fe<sub>3</sub>GeTe<sub>2</sub> [18]. It has been reported that the Fe<sub>3</sub>GeTe<sub>2</sub> has a metallic band structure with a perpendicular magnetic anisotropy of 2.76 meV/cell, and the Curie temperature is 130 K [19,20]. Unlike the Fe<sub>3</sub>GeTe<sub>2</sub>, both CrGeTe<sub>3</sub> and CrI<sub>3</sub> structures have band gaps. In these two systems, the CrI<sub>3</sub> had relatively higher Curie temperature of 45 K with a perpendicular magnetic anisotropy than the CrGeTe<sub>3</sub> (28 K). More interestingly, the CrI<sub>3</sub> shows ferromagnetic (FM) ground state in the odd number of layers while the antiferromagnetic (AFM) state is obtained in the even number of layer system [21]. In our previous work, we also reported that the external pressure can induce a transition from antiferromagnetic to ferromagnetic state in the bilayer with greatly enhanced perpendicular magnetic anisotropy.[13] Thus, the chromium tri-halides CrX<sub>3</sub> (X = Br, Cl) structure has attracted extensive research efforts [22–24].

Very recently, it has been proposed that the 2D FM state can be observed in vanadium tri-iodide ( $\text{VI}_3$ ). Indeed, the bulk  $\text{VI}_3$  displays the Mott insulator nature and also the structural transition from the monoclinic to the rhombohedral structure at 79 K. Moreover, the magnetic phase transition from non-magnetic state to FM state is observed at 50 K. It has also been claimed that the  $\text{VI}_3$  can be easily cleaved into few-layer thickness[25,26]. Despite these interesting physical properties of the bulk  $\text{VI}_3$ , it is rare to find the magnetic properties of the ultrathin  $\text{VI}_3$ . Thus, in this report, we will explore the magnetic properties of monolayer  $\text{VI}_3$ . Particularly, we will focus on the magnetic properties affected by the tensile and compressive strain.

## II. NUMERICAL METHOD

We used the Vienna ab initio simulation package (VASP)[27,28] with the Perdew–Burke–Ernzerhof generalized gradient approximation (GGA)[29] within the framework of projector augmented wave (PAW) method. We also employed the Grimme's DFT-D3 scheme to describe the intralayer van der Waals interactions.[30] The plane wave cut-off energy of 500 eV was used. The Brillouin zone has been sampled by the  $\Gamma$  – centered Monkhorst-Pack method [31] and we used the k-mesh of 11x11x1 for the structural relaxation. The energy and force convergence criterion were set to  $10^{-5}$  eV and  $0.01$  eV  $\text{\AA}^{-1}$ . For magnetic anisotropy, we used denser k-mesh of 21x21x1. A non-collinear total energy calculation with spin orbit coupling was adopted for determining the magnetization direction. To avoid an artificial interaction between the neighboring unit cell, we applied the vacuum distance more than 20  $\text{\AA}$  along the z-axis. For calculating the Curie temperature ( $T_c$ ), we estimated the temperature dependent magnetization curve based on the Metropolis Monte Carlo (MC) simulations using the VAMPIRE software package [32].

## II. NUMERICAL RESULTS

The crystal structure of bulk  $\text{VI}_3$  has two forms; rhombohedral  $\text{R}\bar{3}$  (space group of # 148) with  $\text{BiI}_3$  at low temperature less than 79 K and monoclinic  $\text{C}2/\text{m}$  symmetry (space group of # 12) at high temperature higher than 79 K. The similar temperature dependent structural transition has been found in the transition metal trihalides  $\text{AX}_3$  ( $\text{X} = \text{Cl}, \text{Br}$  and  $\text{I}$ ) family[15,25]. As remarked above, the bulk  $\text{VI}_3$  has a non-magnetic ground state in high temperature phase while the low temperature phase has a ferromagnetic (FM) ground state. Thus, in this report, we consider a monolayer two-

dimensional (2D)  $\text{VI}_3$  in the low temperature structure. Fig. 1(a)-(b) shows the schematic illustration of top and side view of the 2D  $\text{VI}_3$  monolayer. The yellow and brown colors represent the iodine atoms at top and bottom layer while the blue color represents vanadium (V) atoms in the middle layer. Two V atoms are in a honeycomb lattice by edge sharing octahedral with six I atoms in a unit cell. Experimentally, it was measured that the bulk  $\text{VI}_3$  had lattice constants of  $a=b=6.8351 \text{ \AA}$  and  $c=19.96 \text{ \AA}$  [26]. However, the lattice constant can be changed from its bulk value in the reduced dimension. Thus, we fully performed the structure relaxation and obtained the optimized lattice constants of  $a = b = 7.07 \text{ \AA}$ . Note that these are very close to the lattice constants of the 2D  $\text{CrI}_3$  monolayer [33,34]. Since the essential issue in this work is to explore the strain effect on the magnetic property of the monolayer  $\text{VI}_3$ , we considered both biaxial tensile and compressive strains on the monolayer, using the relation  $\varepsilon = \frac{a - a_0}{a_0}$  where  $a_0$  and  $a$  are the equilibrium and stretched or compressed lattice constants. We carefully examined the effect of strain over the bond angles, and the results are presented in Table 1.

We first investigated the magnetic ground state of the 2D  $\text{VI}_3$  monolayer. To explore the magnetic ground state of the monolayer system, we considered three magnetic spin configurations; ferromagnetic (FM), antiferromagnetic (AFM), and non-magnetic (NM). We found that the non-magnetic state was the most unstable by an energy difference of approximately 4 eV compared with the magnetic states. Thus, we present the total energy difference between FM and AFM states ( $\Delta E = E_{\text{AFM}} - E_{\text{FM}}$ ) in Table 1. In the pristine monolayer, the FM state was more stable than the AFM state with an energy difference of 28 meV/cell. Under the tensile strain, we still found FM ground state, and the energy difference was slightly enhanced whereas the energy difference was suppressed under the compressive strain. Overall, we found that the monolayer structure had a FM ground state at least up to  $\pm 3\%$  strain. The calculated magnetic moment was  $4 \mu_B/\text{unit cell}$ , and this was unchanged under the tensile and compressive strains. Since the 2D  $\text{VI}_3$  monolayer had an integer magnetic moment, the monolayer structure may have either half metallic or magnetic semiconducting band structure. Thus, we calculated the electronic band structures. Fig. 2 (a) shows the band structure of the pristine layer. The blue and red lines represent the majority and minority spin bands. The pristine monolayer structure has an indirect band gap of 0.98 eV. Fig. 2(b)-(e) shows the band structures under the tensile and compressive strains. We have found that the band gap is increased (decreased) with tensile (compressive) strain as shown in Table 1, and this is similar to the reports found in many 2D materials [35]. Note that the indirect band gap nature is preserved,

except for 3% compressive strain where the transition from indirect to direct band gap feature appears. We have also investigated the relation between the band gap and bond angles at different tensile/compressive strains. Generally, the band gap has increased with decreasing bond angle whereas it is decreased with increasing bond angle as reported in earlier theoretical works [36,37]. We also calculated the partial density of states (PDOS) of  $\text{VI}_3$  monolayer. Indeed, we found that two V atoms had the same characteristic. In the iodine atom, the iodine atoms indicated by 3 and 6 in Fig. 1(b) had almost the same PDOS while all other iodine atoms had the similar behavior. Thus, we only presented the PDOS of one V atom and the iodine atoms at site 2 and 3. Fig. 3(a) shows the PDOS of the pristine layer. The top panel is the PDOS of the V atom while the middle and bottom panels are for the iodine atom 2 and 3 respectively. As shown, the conduction band minimum (CBM) is constructed by the V d-orbitals whereas the valence band minimum (VBM) is mostly originated from the iodine p-orbitals. The CBM is formed by the  $d_{x^2-y^2}$  and  $d_{xz}$  orbitals whereas the hybridization of  $p_x$  and  $p_y$  orbitals of the iodine atom contributed to the VBM. Fig. 3(b)-(c) shows the PDOS under 1.2 and 3 % tensile strain while Fig. 3(d)-(e) is the PDOS under 1.2 and 3 % compressive strain. Except the 3 % tensile strain, the CBM is still dominated by the hybridization of  $d_{x^2-y^2}$  and  $d_{xz}$  orbitals while the orbital character of the VBM is unchanged.

Table 1: Bond angles, calculated energy difference ( $\Delta E$ ), band gap energies  $E_g$ , magnetocrystalline anisotropy (MAE), exchange magnetic couplings ( $J$ ), and Curie temperature ( $T_c$ ).

Strain (%)	$\Delta E$ (meV)	angle( $^\circ$ ) V <sub>2</sub> -I <sub>1</sub> -I <sub>4</sub>	angle( $^\circ$ ) V <sub>2</sub> -I <sub>3</sub> -I <sub>6</sub>	$E_g$ (eV)	MAE (meV)	$J$ ( $\times 10^{-22}$ J)	$T_c$ (K)
V <sub>2</sub> -I <sub>1</sub> -I <sub>4</sub> V <sub>2</sub> -I <sub>3</sub> -I <sub>6</sub>							
Pristine	28.03	86.91	85.82	0.95	0.29	5.61	46
1.2 %	31.2	85.89	84.36	0.98	0.39	6.23	49
3 %	33.1	84.09	83.83	1.20	0.23	6.65	57
-1.2 %	23.66	84.32	87.82	0.88	0.27	4.74	38
-3 %	20.50	89.40	89.23	0.83	0.20	4.11	35

We now discuss the magnetic anisotropy. To this end, we performed the non-collinear total energy calculations with spin orbit coupling along [100] and [001]. The [100] and [001] magnetic axes are called in-plane and perpendicular magnetization direction. Since the magnitude of the magnetic anisotropy is rather small, it requires more accurate

1  
 2  
 3 energy convergence. We carefully checked the total energy convergence with a dense k-mesh of 21x21x1. The  
 4 calculated magnetic anisotropy energy (MAE) is presented in Table 1. In the pristine layer, we found a perpendicular  
 5 magnetic anisotropy, and the calculated MAE was 0.29 meV/cell. As shown in Table 1, the perpendicular magnetic  
 6 anisotropy was still preserved under the strain although the MAE was changed by the strain. Under the 1.2 % tensile  
 7 strain, it was increased from 0.29 meV to 0.39 meV, but it was slightly suppressed to 0.23 meV at 3 % tensile strain.  
 8 In contrast, it was gradually decreased under the compressive strain. To explore more details, we analyzed the atom  
 9 resolved contribution to the MAE. The purple color represents the contribution to the MAE from the I atoms while  
 10 the blue color shows the contributions from the V atoms. Fig. 4 (a) shows the result in the pristine structure. Both  
 11 vanadium atoms contributed to the perpendicular magnetic anisotropy with MAE of 0.15 meV/atom. On the other  
 12 hand, the iodine atoms had site dependent contribution to the anisotropy. For instance, the iodine atoms at site 3 and  
 13 6 indicated in Fig. 1(a) had in-plane contributions with MAE of 0.15 meV/atom while all other iodine atoms had  
 14 perpendicular magnetic anisotropy although the magnitude of MAE had site dependency. We found that the overall  
 15 contribution from the whole iodine atoms was rather weak due to the opposite contribution, and consequently the  
 16 perpendicular magnetic anisotropy mostly originated from the vanadium atoms. Fig. 4(b) shows the result at 3 %  
 17 biaxial strain. We found that the site dependent contribution to the MAE was considerably changed. For instance, the  
 18 contribution to the perpendicular anisotropy from one of the V atoms was greatly suppressed whereas the  
 19 perpendicular anisotropy from iodine atom at site 4 was substantially enhanced. Meantime, the in-plane contributions  
 20 from site 3 and 6 were suppressed. Thus, we found that the total contributions to the anisotropy from six iodine atoms  
 21 and two vanadium atoms were almost the same. Fig. 4(c) shows the result at 3 % compressive strain. In this case, we  
 22 found that the net contribution from the four iodine atoms was in-plane while the vanadium atoms had perpendicular  
 23 anisotropy. Overall, we found that the contribution to the magnetic anisotropy from each atom was sensitive to the  
 24 strain, but the net effect was rather insensitive to the strain preserving the perpendicular magnetic anisotropy as shown  
 25 in Table 2. Along with the magnetic anisotropy, we also calculated the Curie temperature. To this end, we calculated  
 26 the temperature dependent magnetization curve using the Metropolis Monte Carlo (MC) simulation with the  
 27 VAMPIRE software package and extracted the Curie temperature ( $T_c$ ). To calculate the Curie temperature ( $T_c$ ), we  
 28 used the classical spin Heisenberg model which can be written  
 29  
 30  
 31  
 32  
 33  
 34  
 35  
 36  
 37  
 38  
 39  
 40  
 41  
 42  
 43  
 44  
 45  
 46  
 47  
 48  
 49  
 50  
 51  
 52  
 53  
 54  
 55  
 56  
 57  
 58  
 59  
 60

$$H = - \sum JM_i M_j$$

where  $J$  is the exchange energy parameter of the first nearest neighbor atom. The  $M_i$  and  $M_j$  are the magnetic moment at site  $i$  and  $j$ . The exchange energy parameter  $J$  can be obtained by the relation  $J = \frac{\Delta E}{NM^2}$  where  $N$  and  $M$  are the total number of magnetic atoms per unit cell and magnetic moment of a single magnetic atom in the unit cell. Further, from equation for calculating exchange energy parameter, we know that as the change in ferromagnetic and anti-ferromagnetic energy results a direct change in the Curie temperature as can be seen in Table and Fig. 5 (a)-(c) respectively. For MC simulations, we considered a large enough supercell of  $50 \times 50$ . Note that the bulk  $\text{VI}_3$  has Curie temperature of 50 K. By using the above quantities, we calculated the temperature dependent magnetization curve, and Fig. 5 (a)-(c) shows the results for pristine and strained systems respectively. Note that the magnetization curve was fitted by using the Curie-Bloch equation in the classical limit as given below

$$m(T) = \left[1 - \frac{T}{T_c}\right]^\beta.$$

In the monolayer structure, the  $T_c$  of the pristine monolayer was 47 K. To check the reliability of our numerical method, we also calculated the  $T_c$  of  $\text{CrI}_3$  and found that our calculated values are close to the previously available reports [38,39]. In Fig. 5(b)-(c), we presented the  $T_c$  at  $\pm 3\%$ . From the Table 1 and Fig. 5(b)-(c), we found that the Curie temperature was increased (decreased) under the tensile (compressive) strain. This is mostly due to the change in the exchange coupling parameter with tensile and compressive strain. Indeed, we have found that the dominant contribution to ferromagnetism in  $\text{VI}_3$  is mainly due to indirect exchange interaction between two V atoms via I atom. Under the strain, the bond angle is changed and the enhancement in the Curie temperature under tensile strain can be explained by the Goodenough-Kanamori-Anderson rule.

## CONCLUSION

In summary, we explored the magnetic properties of the 2D  $\text{VI}_3$  monolayer using the density functional theory (DFT). We found that the 2D monolayer structure had slightly larger lattice constant than the bulk value. The pristine monolayer structure had an indirect band gap of 0.98 eV and the total magnetic moment was  $4 \mu_B$  per unit cell. Under the tensile and compressive strains, the essential band structure was not changed although the band gap was slightly

increased (decreased) under the tensile (compressive) strain. We also calculated the magnetic anisotropy of the monolayer system. The pristine layer had a perpendicular magnetic anisotropy, and the calculated magnetic anisotropy energy was 0.29 meV/cell. It was found that the strain had no significant effect on the net perpendicular magnetic anisotropy energy although the contribution to the anisotropy from an individual atom was affected by the external strain. Through the temperature dependent magnetization curve calculations, we obtained that the monolayer had a T<sub>c</sub> of 46 K. This Curie temperature was increased to 57 K at 3 % tensile strain whereas it was decreased to 35 K at 3 % compressive strain. Overall, we found that the magnetic properties of the 2D monolayer structure was robust under the strain at least up to  $\pm 3\%$  the tensile/compressive strain.

## AUTHOR INFORMATION

### Corresponding Authors

\*E-mail: [hongj@pknu.ac.kr](mailto:hongj@pknu.ac.kr)

### Conflict of interest

The authors have no conflict of interest.

### Acknowledgments

This research was supported by the Basic Science Research Program through the National Research Foundation of Korea (NRF) funded by the Ministry of Science, ICT and Future Planning ([2019RA21B5B01069807](https://doi.org/10.1007/s11012-019-00698-0)).

### References

- [1] K.S. Novoselov, A.K. Geim, S.V. Morozov, D. Jiang, Y. Zhang, S.V. Dubonos, I.V. Grigorieva, A.A. Firsov, Electric field effect in atomically thin carbon films, *Science*. 306 (2004) 666–669.  
<https://doi.org/10.1126/science.1102896>.
- [2] A. Falin, Q. Cai, E.J.G. Santos, D. Scullion, D. Qian, R. Zhang, Z. Yang, S. Huang, K. Watanabe, T. Taniguchi, M.R. Barnett, Y. Chen, R.S. Ruoff, L.H. Li, Mechanical properties of atomically thin boron nitride and the role of interlayer interactions, *Nat. Commun.* 8 (2017) 1–9.  
<https://doi.org/10.1038/ncomms15815>.

- [3] P. Vogt, P. De Padova, C. Quaresima, J. Avila, E. Frantzeskakis, M.C. Asensio, A. Resta, B. Ealet, G. Le Lay, Silicene: Compelling Experimental Evidence for Graphenelike Two-Dimensional Silicon, *Phys. Rev. Lett.* 108 (2012) 155501. <https://doi.org/10.1103/PhysRevLett.108.155501>.
- [4] T. Shen, A.V. Penumatcha, J. Appenzeller, Strain Engineering for Transition Metal Dichalcogenides Based Field Effect Transistors, *ACS Nano.* 10 (2016) 4712–4718. <https://doi.org/10.1021/acsnano.6b01149>.
- [5] C.R. Dean, A.F. Young, I. Meric, C. Lee, L. Wang, S. Sorgenfrei, K. Watanabe, T. Taniguchi, P. Kim, K.L. Shepard, J. Hone, Boron nitride substrates for high-quality graphene electronics, *Nat. Nanotechnol.* 5 (2010) 722–726. <https://doi.org/10.1038/nnano.2010.172>.
- [6] S. Cahangirov, M. Topsakal, E. Aktürk, H. Şahin, S. Ciraci, Two- and One-Dimensional Honeycomb Structures of Silicon and Germanium, *Phys. Rev. Lett.* 102 (2009) 236804. <https://doi.org/10.1103/PhysRevLett.102.236804>.
- [7] K.F. Mak, C. Lee, J. Hone, J. Shan, T.F. Heinz, Atomically Thin MoS<sub>2</sub>: A New Direct-Gap Semiconductor, *Phys. Rev. Lett.* 105 (2010) 136805. <https://doi.org/10.1103/PhysRevLett.105.136805>.
- [8] Q.H. Wang, K. Kalantar-Zadeh, A. Kis, J.N. Coleman, M.S. Strano, Electronics and optoelectronics of two-dimensional transition metal dichalcogenides, *Nat. Nanotechnol.* 7 (2012) 699–712. <https://doi.org/10.1038/nnano.2012.193>.
- [9] L. Li, Y. Yu, G.J. Ye, Q. Ge, X. Ou, H. Wu, D. Feng, X.H. Chen, Y. Zhang, Black phosphorus field-effect transistors, *Nat. Nanotechnol.* 9 (2014) 372–377. <https://doi.org/10.1038/nnano.2014.35>.
- [10] F. Subhan, M.U. Farooq, J. Hong, Bias-dependent transport properties of passivated tilted black phosphorene nanoribbons, *Phys. Chem. Chem. Phys.* 20 (2018) 11021–11027. <https://doi.org/10.1039/C8CP00090E>.
- [11] E.M.D. Siriwardane, D. Çakir, Strain engineering of electronic and magnetic properties of double-transition metal ferromagnetic semiconductor MXenes, *J. Appl. Phys.* 125 (2019) 082527. <https://doi.org/10.1063/1.5054131>.
- [12] T. Song, Z. Fei, M. Yankowitz, Z. Lin, Q. Jiang, K. Hwangbo, Q. Zhang, B. Sun, T. Taniguchi, K. Watanabe, M.A. McGuire, D. Graf, T. Cao, J.-H. Chu, D.H. Cobden, C.R. Dean, D. Xiao, X. Xu, Switching 2D magnetic states via pressure tuning of layer stacking, *Nat. Mater.* 18 (2019) 1298–1302. <https://doi.org/10.1038/s41563-019-0505-2>.
- [13] F. Subhan, I. Khan, J. Hong, Pressure-induced ferromagnetism and enhanced perpendicular magnetic anisotropy of bilayer CrI<sub>3</sub>, *J. Phys. Condens. Matter.* 31 (2019) 355001. <https://doi.org/10.1088/1361-648X/ab2308>.
- [14] B. Huang, G. Clark, E. Navarro-Moratalla, D.R. Klein, R. Cheng, K.L. Seyler, D. Zhong, E. Schmidgall, M.A. McGuire, D.H. Cobden, W. Yao, D. Xiao, P. Jarillo-Herrero, X. Xu, Layer-dependent ferromagnetism in a van der Waals crystal down to the monolayer limit, *Nature.* 546 (2017) 270–273. <https://doi.org/10.1038/nature22391>.
- [15] M.A. McGuire, H. Dixit, V.R. Cooper, B.C. Sales, Coupling of Crystal Structure and Magnetism in the Layered, Ferromagnetic Insulator CrI<sub>3</sub>, *Chem. Mater.* 27 (2015) 612–620. <https://doi.org/10.1021/cm504242t>.
- [16] N. Richter, D. Weber, F. Martin, N. Singh, U. Schwingenschlögl, B.V. Lotsch, M. Kläui, Temperature-dependent magnetic anisotropy in the layered magnetic semiconductors CrI<sub>3</sub> and CrBr<sub>3</sub>, *Phys. Rev. Mater.* 2 (2018) 024004. <https://doi.org/10.1103/PhysRevMaterials.2.024004>.
- [17] C. Xu, J. Feng, H. Xiang, L. Bellaiche, Interplay between Kitaev interaction and single ion anisotropy in ferromagnetic CrI<sub>3</sub> and CrGeTe<sub>3</sub> monolayers, *Npj Comput. Mater.* 4 (2018) 1–6. <https://doi.org/10.1038/s41524-018-0115-6>.

- [18] Z. Fei, B. Huang, P. Malinowski, W. Wang, T. Song, J. Sanchez, W. Yao, D. Xiao, X. Zhu, A.F. May, W. Wu, D.H. Cobden, J.-H. Chu, X. Xu, Two-dimensional itinerant ferromagnetism in atomically thin Fe<sub>3</sub>GeTe<sub>2</sub>, *Nat. Mater.* 17 (2018) 778–782. <https://doi.org/10.1038/s41563-018-0149-7>.
- [19] Z. Fei, B. Huang, P. Malinowski, W. Wang, T. Song, J. Sanchez, W. Yao, D. Xiao, X. Zhu, A.F. May, W. Wu, D.H. Cobden, J.-H. Chu, X. Xu, Two-dimensional itinerant ferromagnetism in atomically thin Fe<sub>3</sub>GeTe<sub>2</sub>, *Nat. Mater.* 17 (2018) 778–782. <https://doi.org/10.1038/s41563-018-0149-7>.
- [20] H.L. Zhuang, P.R.C. Kent, R.G. Hennig, Strong anisotropy and magnetostriction in the two-dimensional Stoner ferromagnet Fe<sub>3</sub>GeTe<sub>2</sub>, *Phys. Rev. B* 93 (2016) 134407. <https://doi.org/10.1103/PhysRevB.93.134407>.
- [21] B. Huang, G. Clark, D.R. Klein, D. MacNeill, E. Navarro-Moratalla, K.L. Seyler, N. Wilson, M.A. McGuire, D.H. Cobden, D. Xiao, W. Yao, P. Jarillo-Herrero, X. Xu, Electrical control of 2D magnetism in bilayer CrI<sub>3</sub>, *Nat. Nanotechnol.* 13 (2018) 544–548. <https://doi.org/10.1038/s41565-018-0121-3>.
- [22] S. Jiang, L. Li, Z. Wang, K.F. Mak, J. Shan, Controlling magnetism in 2D CrI<sub>3</sub> by electrostatic doping, *Nat. Nanotechnol.* 13 (2018) 549–553. <https://doi.org/10.1038/s41565-018-0135-x>.
- [23] M. Moaied, J. Lee, J. Hong, A 2D ferromagnetic semiconductor in monolayer Cr-trihalide and its Janus structures, *Phys. Chem. Chem. Phys.* 20 (2018) 21755–21763. <https://doi.org/10.1039/C8CP03489C>.
- [24] J. Liu, Q. Sun, Y. Kawazoe, P. Jena, Exfoliating biocompatible ferromagnetic Cr-trihalide monolayers, *Phys. Chem. Chem. Phys.* 18 (2016) 8777–8784. <https://doi.org/10.1039/C5CP04835D>.
- [25] T. Kong, K. Stolze, E.I. Timmons, J. Tao, D. Ni, S. Guo, Z. Yang, R. Prozorov, R.J. Cava, VI<sub>3</sub>—a New Layered Ferromagnetic Semiconductor, *Adv. Mater.* 31 (2019) 1808074. <https://doi.org/10.1002/adma.201808074>.
- [26] S. Tian, J.-F. Zhang, C. Li, T. Ying, S. Li, X. Zhang, K. Liu, H. Lei, Ferromagnetic van der Waals Crystal VI<sub>3</sub>, *J. Am. Chem. Soc.* 141 (2019) 5326–5333. <https://doi.org/10.1021/jacs.8b13584>.
- [27] G. Kresse, J. Furthmüller, Efficient iterative schemes for ab initio total-energy calculations using a plane-wave basis set, *Phys. Rev. B* 54 (1996) 11169–11186. <https://doi.org/10.1103/PhysRevB.54.11169>.
- [28] G. Kresse, J. Furthmüller, Efficiency of ab-initio total energy calculations for metals and semiconductors using a plane-wave basis set, *Comput. Mater. Sci.* 6 (1996) 15–50. [https://doi.org/10.1016/0927-0256\(96\)00008-0](https://doi.org/10.1016/0927-0256(96)00008-0).
- [29] J.P. Perdew, K. Burke, M. Ernzerhof, Generalized Gradient Approximation Made Simple, *Phys. Rev. Lett.* 77 (1996) 3865–3868. <https://doi.org/10.1103/PhysRevLett.77.3865>.
- [30] S. Grimme, J. Antony, S. Ehrlich, H. Krieg, A consistent and accurate ab initio parametrization of density functional dispersion correction (DFT-D) for the 94 elements H-Pu, *J. Chem. Phys.* 132 (2010) 154104. <https://doi.org/10.1063/1.3382344>.
- [31] H.J. Monkhorst, J.D. Pack, Special points for Brillouin-zone integrations, *Phys. Rev. B* 13 (1976) 5188–5192. <https://doi.org/10.1103/PhysRevB.13.5188>.
- [32] R.F.L. Evans, W.J. Fan, P. Chureemart, T.A. Ostler, M.O.A. Ellis, R.W. Chantrell, Atomistic spin model simulations of magnetic nanomaterials, *J. Phys. Condens. Matter.* 26 (2014) 103202. <https://doi.org/10.1088/0953-8984/26/10/103202>.
- [33] L. Webster, J.-A. Yan, Strain-tunable magnetic anisotropy in monolayer CrCl<sub>3</sub>, CrBr<sub>3</sub>, and CrI<sub>3</sub>, *Phys. Rev. B* 98 (2018) 144411. <https://doi.org/10.1103/PhysRevB.98.144411>.
- [34] J.L. Lado, J. Fernández-Rossier, On the origin of magnetic anisotropy in two dimensional CrI<sub>3</sub>, *2D Mater.* 4 (2017) 035002. <https://doi.org/10.1088/2053-1583/aa75ed>.

- [35] L.M. Sandonas, R. Gutierrez, A. Pecchia, G. Seifert, G. Cuniberti, Tuning quantum electron and phonon transport in two-dimensional materials by strain engineering: a Green's function based study, *Phys. Chem. Chem. Phys.* 19 (2017) 1487–1495. <https://doi.org/10.1039/C6CP06621F>.
- [36] P. Johari, V.B. Shenoy, Tuning the Electronic Properties of Semiconducting Transition Metal Dichalcogenides by Applying Mechanical Strains, *ACS Nano.* 6 (2012) 5449–5456. <https://doi.org/10.1021/nn301320r>.
- [37] E. Scalise, M. Houssa, G. Pourtois, V. Afanas'ev, A. Stesmans, Strain-induced semiconductor to metal transition in the two-dimensional honeycomb structure of MoS<sub>2</sub>, *Nano Res.* 5 (2012) 43–48. <https://doi.org/10.1007/s12274-011-0183-0>.
- [38] P. Jiang, L. Li, Z. Liao, Y.X. Zhao, Z. Zhong, Spin Direction-Controlled Electronic Band Structure in Two-Dimensional Ferromagnetic CrI<sub>3</sub>, *Nano Lett.* 18 (2018) 3844–3849. <https://doi.org/10.1021/acs.nanolett.8b01125>.
- [39] X. Li, J. Yang, CrXTe<sub>3</sub> (X = Si, Ge) nanosheets: two dimensional intrinsic ferromagnetic semiconductors, *J. Mater. Chem. C.* 2 (2014) 7071–7076. <https://doi.org/10.1039/C4TC01193G>.

## Figure Captions

**Figure 1.** (a) Top and (b) side view of VI<sub>3</sub> monolayer unit cell. The red dashed color shows the unit cell of VI<sub>3</sub> monolayer.

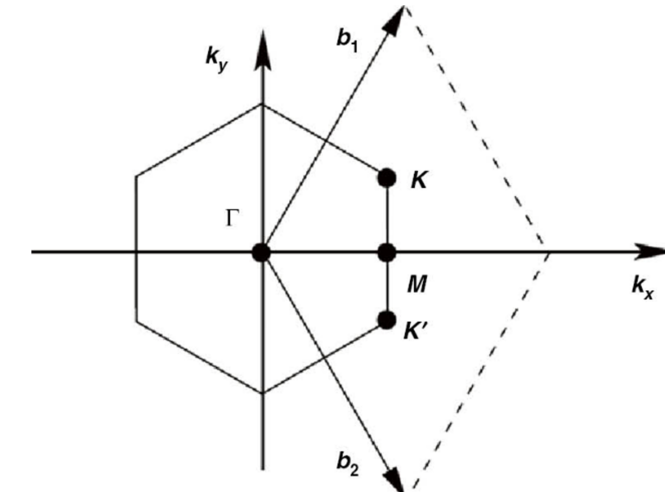
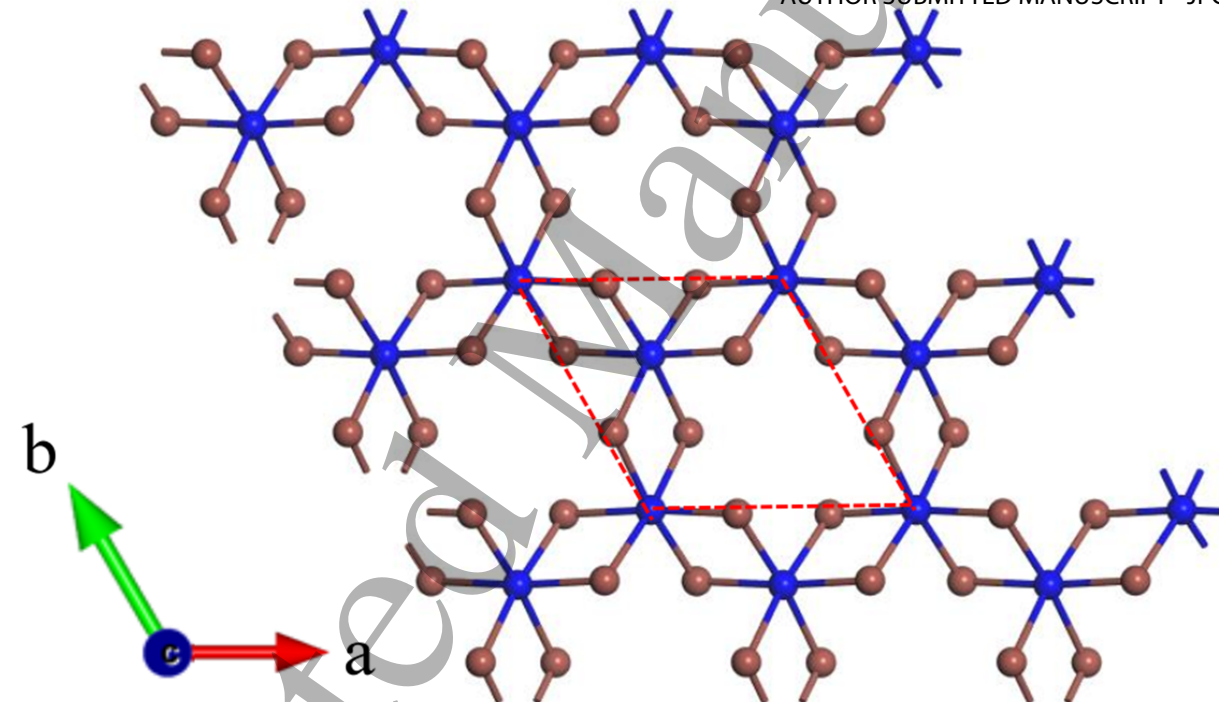
**Figure 2.** Band structures at (a) 0, (b) 1.2, (c) 3, (d) -1.2 and (e) -3 % biaxial strain of VI<sub>3</sub> monolayer.

**Figure 3.** Partial DOS of (a) 0, (b) 1.2, (c) 3, (d) -1.2 and (e) -3 % biaxial strain of VI<sub>3</sub> monolayer. The upper panel is for V atoms and the lower two panels are for I atoms respectively.

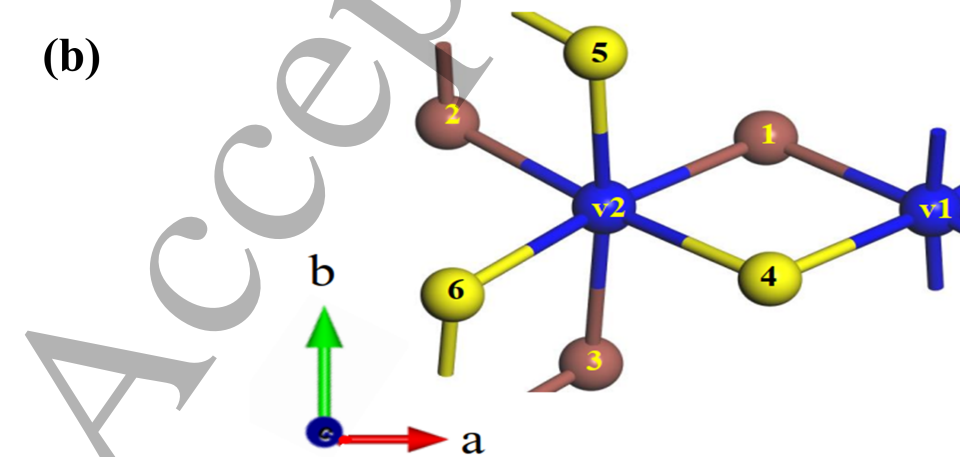
**Figure 4.** Atomic and site specified contribution to MAE of (a) 0, (b) 3, and (c) -3 % biaxial strain of VI<sub>3</sub> monolayer.

**Figure 5:** Curie temperature at (a) 0, (b) 3, and (c) -3% strain of VI<sub>3</sub> monolayer.

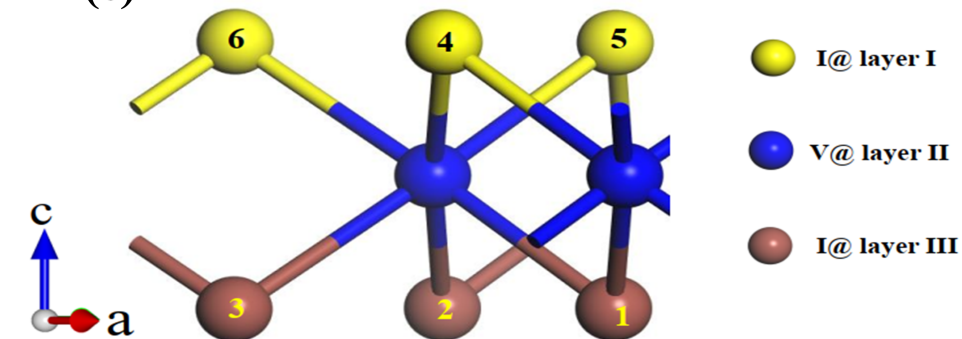
(a)



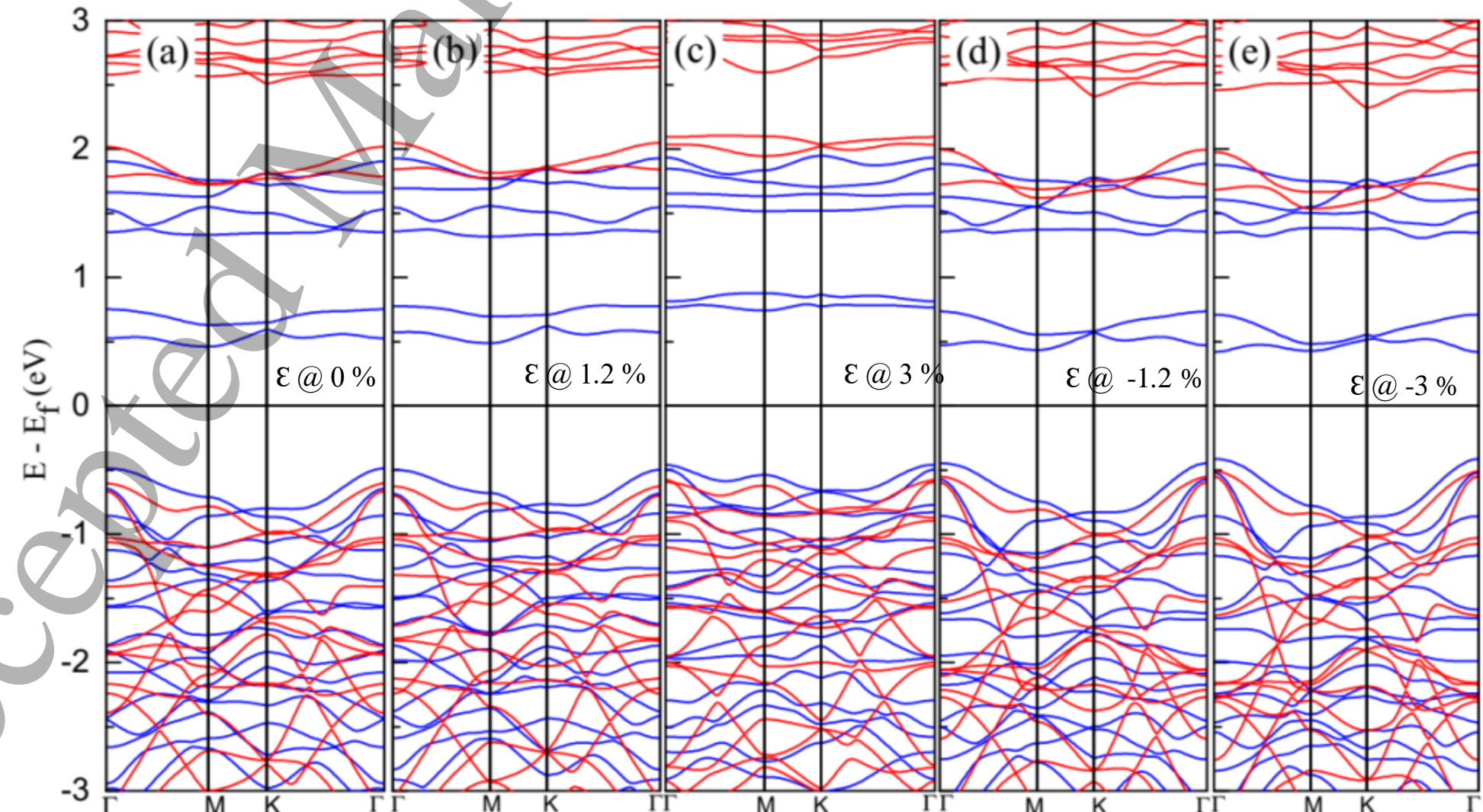
(b)

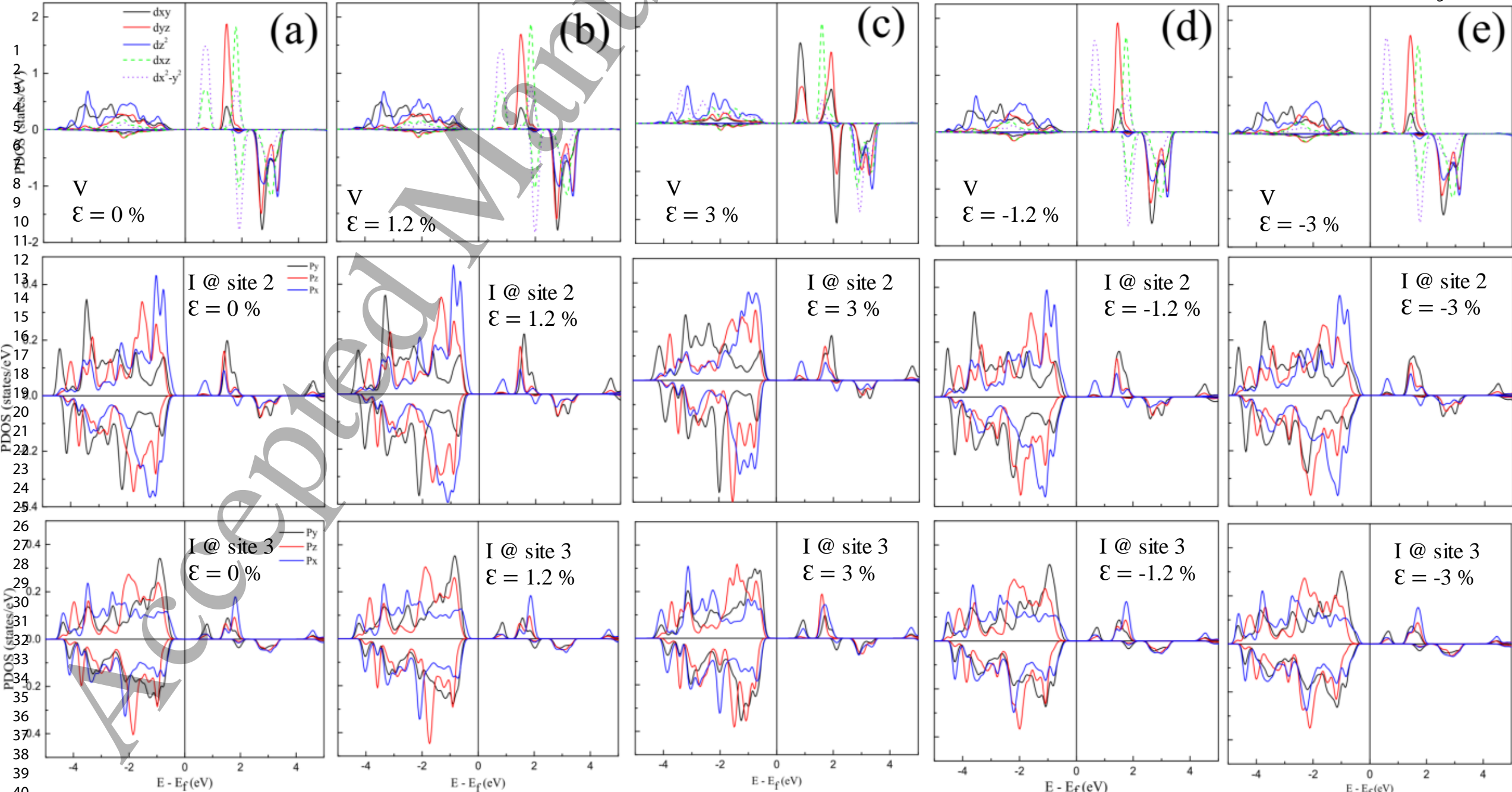


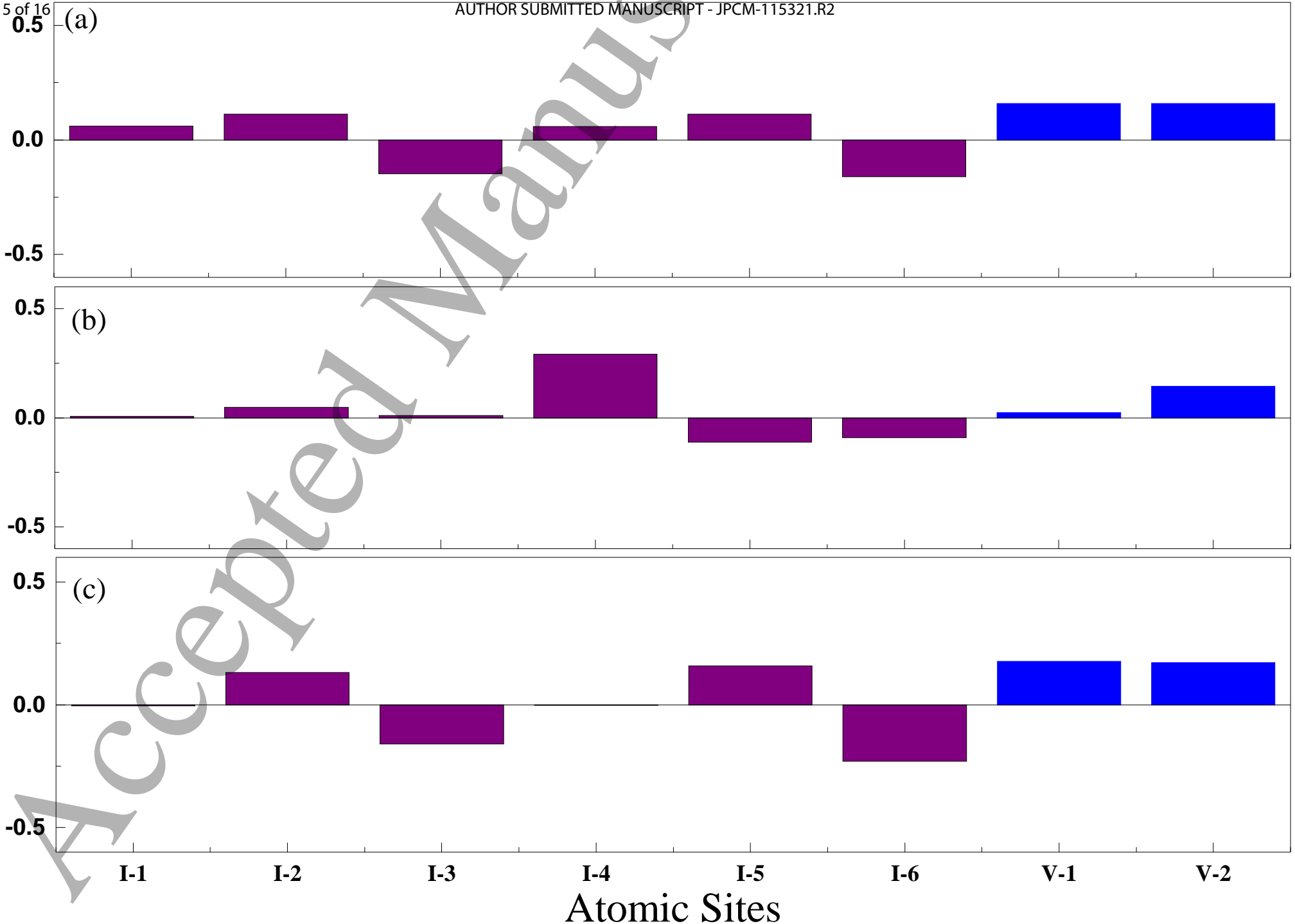
(c)

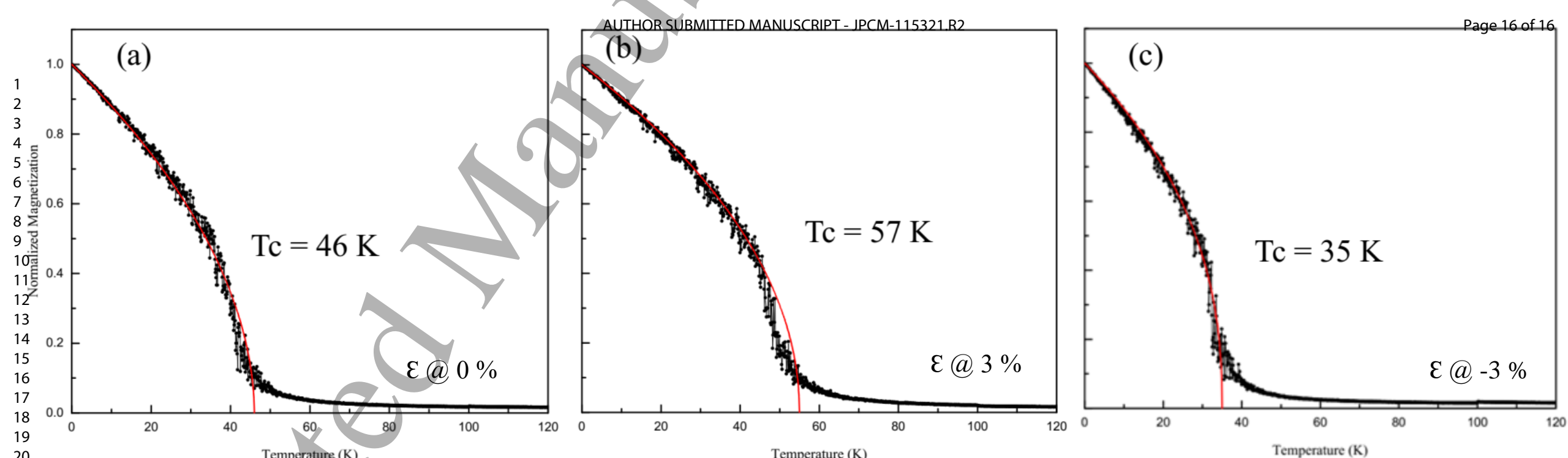


- $I @ \text{layer I}$
- $V @ \text{layer II}$
- $I @ \text{layer III}$









20  
21  
22  
23  
24  
25  
26  
27  
28  
29  
30  
31  
32  
33  
34  
35  
36  
37  
38  
39  
40  
41